JOC The Journal of Organic Chemistry

Article

pubs.acs.org/joc

Mechanisms and Transition States of 1,3-Dipolar Cycloadditions of Phenyl Azide with Enamines: A Computational Analysis

Steven A. Lopez,[‡] Morton E. Munk,[†] and K. N. Houk*[,‡]

[‡]Department of Chemistry and Biochemistry, University of California, Los Angeles, California 90095-1569, United States

[†]Department of Chemistry and Biochemistry, Arizona State University, Tempe, Arizona 85287, United States

Supporting Information

ABSTRACT: The transition structures for the 1,3-dipolar cycloadditions of phenyl azide to enamines derived from acetophenone or phenylacetaldehyde and piperidine, morpholine, or pyrrolidine were located using quantum mechanical methods. These cycloadditions were studied experimentally in 1975 by Meilahn, Cox, and Munk (*J. Org. Chem.* **1975**, *40*, 819−823). Calculations were carried out with M06-2X/6-311+G(d,p), SCS-MP2/6-311+G(d,p)//M06-2X/6-311+G(d,p), and B97D/6-311+G(d,p) methods with the IEF-PCM solvation model for chloroform and ethanol. The distortion/interaction model was utilized to understand mechanisms, reactivities, and selectivities.

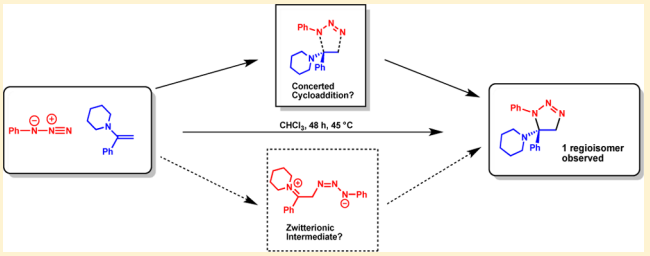

INTRODUCTION

The "click" reactions of azides with terminal alkynes catalyzed by copper catalysts, and the copper free analogs involving azides and strained alkynes, have attracted much attention in the past decade due to a great variety of applications in chemical biology and materials chemistry.[1−5] These reactions involve two reaction partners, neither of which is electrophilic or nucleophilic with respect to the other. Either copper catalysis or strain-induced activation (distortion-accelerated reactions) are required to achieve acceptable rates.[6,7]

This paper describes a theoretical exploration of a different type of azide cycloaddition, involving very nucleophilic enamines that react rapidly with the relatively electrophilic azides. Through measurements of solvent effects on rate constants, Hammett parameters, and semiempirical Complete Neglect of Differential Overlap (CNDO) molecular orbital calculations, Munk et al. deduced that the reactions involve a concerted mechanism with highly asynchronous transition states.[8]

We have employed quantum mechanical calculations to characterize the reaction mechanism and transition states for such processes. We previously investigated simple enamine−azide (3 + 2) cycloadditions to look for reversible reactions that might be candidates for Dynamic Combinatorial Chemistry.[9] We now report on the 1,3-dipolar cycloadditions of phenyl azide to the enamines derived from acetophenone and piperidine (**1a**), pyrrolidine (**1b**), and morpholine (**1c**), or phenylacetylaldehyde and piperidine (**2**) (Scheme 1).

The reactions of 1,1-disubstituted enamines (**1a−c**) and *trans*-enamine (**2**) with phenyl azide and the possible products are shown in Figure 1. Munk et al. performed the reactions and found that **3a−c** and **5** were formed exclusively. The reactions were performed in chloroform, ethanol, and acetonitrile, and only minor variations in reaction rates were observed.[8] We have investigated the mechanisms and regioselectivities of the enamine−azide cycloadditions studied by Munk. The distortion/interaction model has been used to provide more complete understanding of the mechanisms and factors controlling reactivities in enamine−azide cycloadditions.[10]

Scheme 1. Enamine Dipolarophiles (1a−c) and 2 Studied by Munk[8] and in This Work

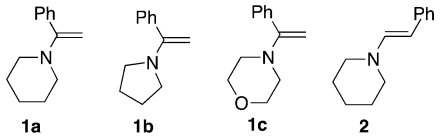

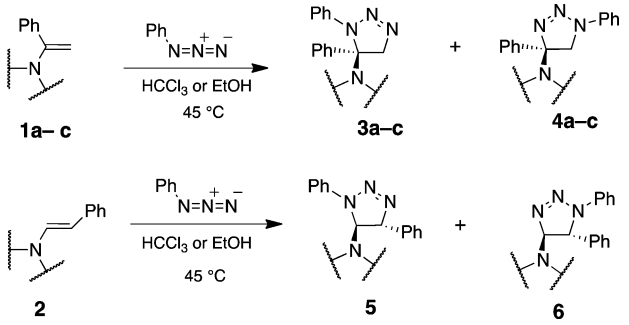

Figure 1. Enamines **1a−c** and **2** undergo reactions with phenyl azide to form **3a−c** and **5**. **4a−c** and **6** are not observed experimentally.

Received: December 11, 2012
Published: January 23, 2013

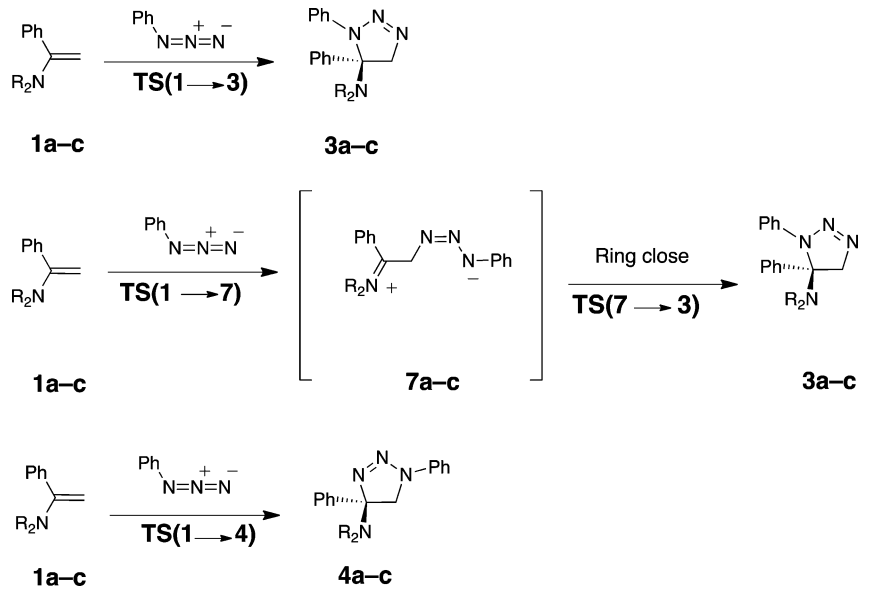

Figure 2. Concerted mechanism of cycloadditions of PhN_3 to enamines **1a–c** and stepwise pathway for formation of **3a–c**.

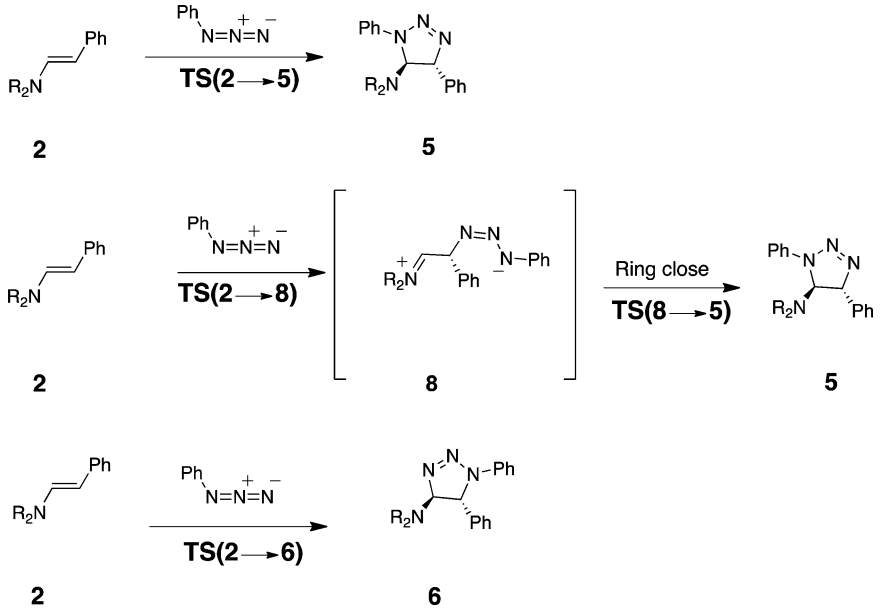

Figure 3. Concerted mechanism of cycloadditions of PhN_3 to enamines **2** and stepwise pathway for formation of **5**.

■ COMPUTATIONAL METHODS

All computations were carried out with the GAUSSIAN 09 series of programs.[11] Reactants, transition states, and products were optimized with M06-2X[12] and B97D[13] methods. The B97D method was used because of its relatively low cost, and the stationary points were reoptimized with M06-2X. Vibrational analysis confirmed all stationary points to be minima (no imaginary frequencies) or first-order saddle points (one imaginary frequency). An ultrafine grid was used with the M06-2X/6-311+G(d,p) geometry optimization. Frequency calculations on these stationary points provided activation enthalpies and free energies. Additional electronic energies were calculated with SCS-MP2[14]/6-311+G(d,p)//M06-2X/6-311+G(d,p) (energies in Supporting Information). The use of solvent was critical in locating stationary points for the stepwise transition structures and intermediates. Polarizable continuum model IEF-PCM[15] for solvation by ethanol and chloroform was used for the computations. The CPCM model was also used to compare activation barriers and obtained similar results[16,17] (Supporting Information). A quasiharmonic correction was applied during the entropy calculations by setting all frequencies to 100 cm^{-1} when they are less than 100 cm^{-1}.[18,19]

■ RESULTS/DISCUSSION

Mechanisms of Azide Cycloadditions to Piperidine Enamines. We have computed both concerted and stepwise paths for the four enamine–azide cycloadditions shown in Figure 1. Both concerted (**a**, Figures 2 and 3) and stepwise (**b**, Figures 2 and 3) pathways were found for formation of observed products **3a–c** and **5**. Only concerted pathways **c** were found for the unobserved product.

The computed transition structures for the reaction of **1a** and **2** are shown in Figure 4. **TS(1a→3a)** and **TS(2→5)** are concerted, although highly asynchronous leading to **3a** and **5**. **TS(1a→4a)** and **TS(2→6)** are concerted and quite synchronous but higher in energy (Figure 6); these lead to the unobserved cycloadducts, **4a** and **6**. The transition structures

dx.doi.org/10.1021/jo302695n | J. Org. Chem. 2013, 78, 1576–1582

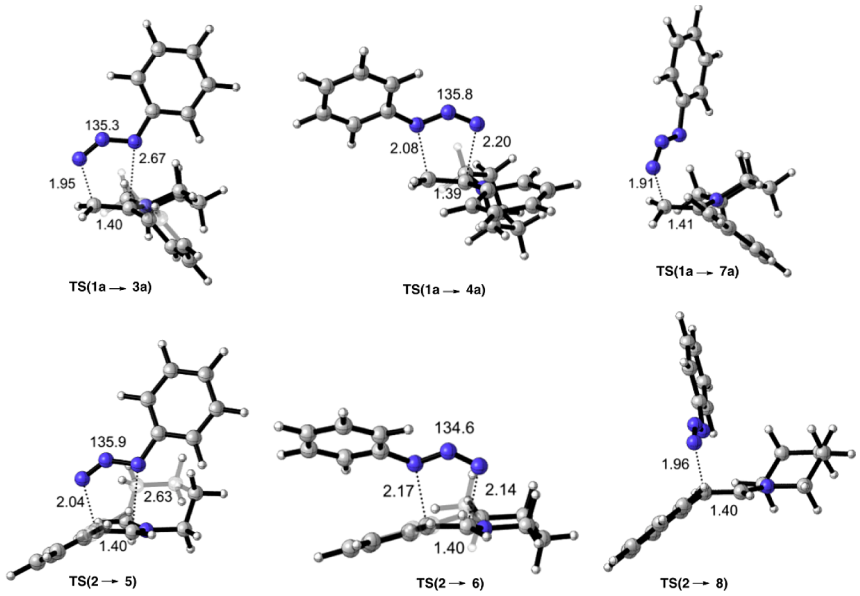

Figure 4. Three possible transition structures for the reactions of **1a−c** and **2** with phenyl azide as calculated by M06-2X/6-311+G(d,p) using IEF-PCM: $CHCl_3$. Bond lengths are in Å.

for the first steps of the stepwise mechanisms **TS(1a→7a)** and **TS(2→8)** result in zwitterionic intermediates, **7a** and **8** (Figure 5). The NNCC dihedral angle in **TS(1a→7a)** is 61.6°.

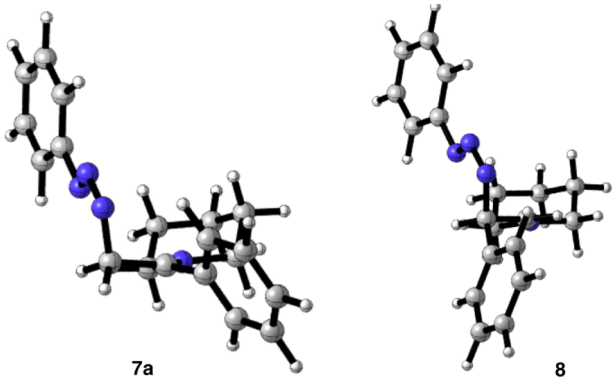

Figure 5. Optimized structures of zwitterionic **7a** and **8** by M06-2X/6-31+G(d,p) IEF-PCM: $CHCl_3$.

Zwitterionic intermediates have been reported by Huisgen[20] and recently by Banert.[21] No transition state could be found for the ring closure to the products, **3a** and **5**, presumably because of the very flat surface region of the zwitterionic intermediates (see below).

The partial double bonds from the enamine substructure are very similar in the transition structures shown in Figure 4 (1.39−1.41 Å) as are the azide bond angles (135°−136°). **TS(1a→3a)** and **TS(2→5)** have transition state bond lengths between the β-carbon and terminal azide nitrogen that are more developed than the other forming bond [1.95 Å vs 2.67 Å for **TS(1a→3a)** and 2.04 Å vs 2.63 Å for **TS(2→5)**]. Based on these bond lengths, the corresponding asynchronicities are 0.72 and 0.59 Å. The transition states leading to the unobserved cycloadducts [**TS(1a→4a)** and **TS(2→6)**] also have very similar enamine double bond lengths (1.39 and 1.40 Å, respectively). These transition states are calculated to have more synchronous bond formation. **TS(1a→4a)** has a slightly more fully formed bond between the β-carbon and the substituted azide terminus (2.08 Å) than does **TS(2→6)** (2.17 Å). The other forming bonds are similar in **TS(1a→4a)** and **TS(2→6)** (2.20 and 2.14 Å, respectively).

The bond-forming step in the stepwise pathways **TS(1a→7a)** and **TS(2→8)** have relatively short CN bonds (1.91 and 1.96 Å, respectively) in line with stepwise cycloadditions. The free energies (kcal mol^{-1}) of transition structures, intermediates, and products resulting from this mechanistic study are shown in Figure 6.

The lowest energy transition states for the reactions of enamines **1a** and **2** with phenyl azide involve highly asynchronous formation of the two bonds as shown in Figure 4. **TS(1a→3a)** and **TS(2→5)** are 11 and 7 kcal mol^{-1} more stable than **TS(1a→4a)**and **TS(2→6)**, respectively. **TS(1a→7a)** and **TS(2→8)** are disfavored by 1.1 and 4.5 kcal mol^{-1}, respectively, and lead to zwitterionic intermediates, **7a** and **8**. Scans of the dihedral angles formed by C−C−N−N in **7a** and **8**, leading to products, **3a** and **5**, are shown in Figure 7. The scans reveal that the potential energy is relatively flat near zwitterionic intermediates **7a** and **8**. The zwitterionic mechanism requires rotation around the dihedral angle (C−C−N−N) until the termini of the azide and alkene interact, at which point the energy drops rapidly to form the second C−N bond. Although no ring closing transition state could be found on the potential energy surface, bond formation is stepwise.

Table 1 shows the free energy activation barriers derived from the experimental rate constants for the reactions studied by Munk et al. using transition state theory (see Supporting Information). The computed barriers of those reactions are given for comparison. M06-2X and SCS-MP2 generally predict activation barriers higher than experimental ones and give the correct order of reactivity. Although B97D incorrectly predicts the order of reactivity if all four reactions in Table 1 are considered, $\Delta G^{\ddagger}$ are in the correct order for the three structurally related acetophenone enamines, **1a−c**. SCS-MP2 and M06-2X predict the correct order of reactivity for **1a−c**. SCS-MP2 and M06-2X incorrectly predict the activation barrier of **1c** to be higher than that of **2**, but the difference is within experimental error. M06-2X predicts barriers 3−4 kcal mol^{-1}

dx.doi.org/10.1021/jo302695n | J. Org. Chem. 2013, 78, 1576−1582

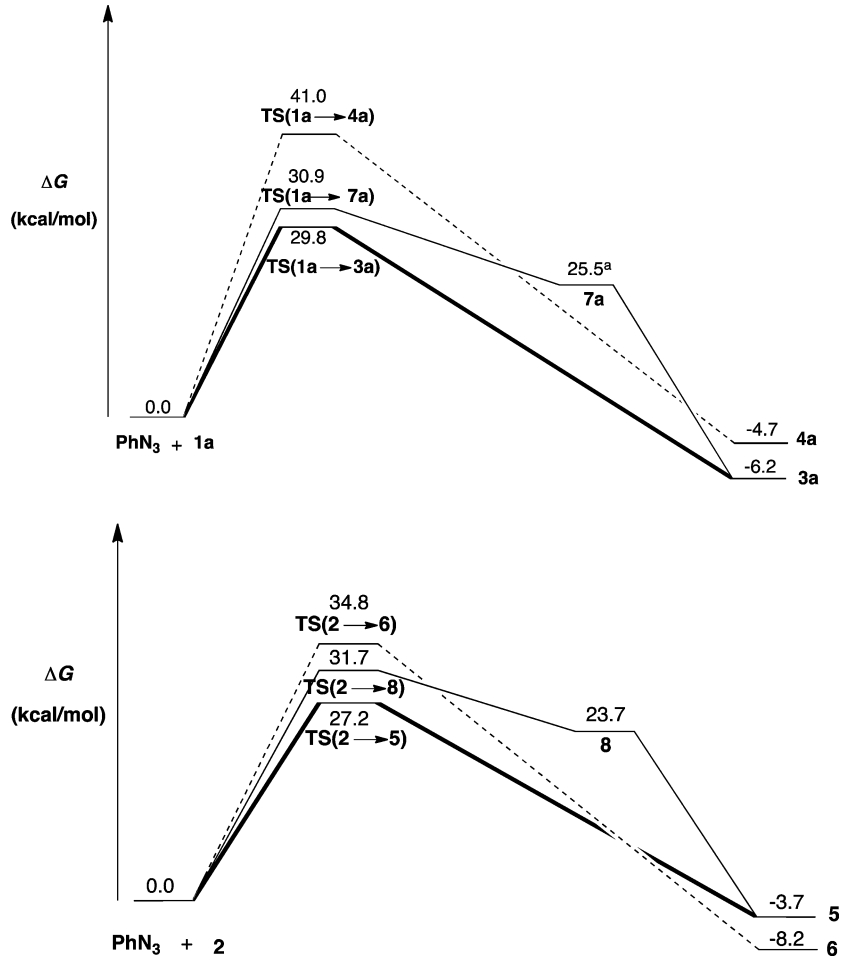

Figure 6. Free energy profile for the cycloadditions of **1a** with PhN_3 and **2** with PhN_3. All stationary points are optimized at the M06-2X/6-311+G(d,p) level of theory with solvation IEF-PCM: $CHCl_3$. [a] **7a** energy is calculated as a single-point M06-2X/6-311+G(d,p)//M06-2X/6-31+G(d) at 44.8 °C with IEF-PCM: $CHCl_3$. Values are in kcal mol^{-1}.

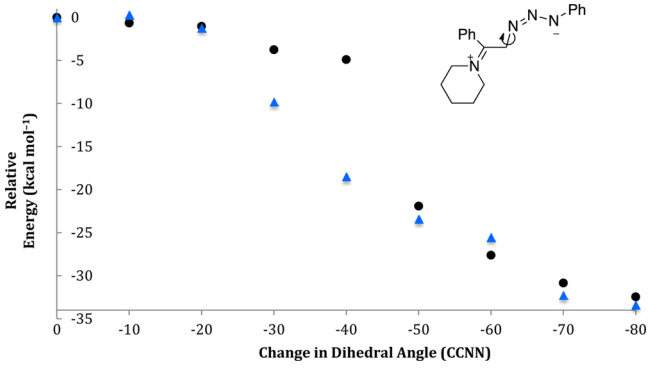

Figure 7. Dihedral angle scan of the ring closing from **7a** (black circle) and **8** (blue triangle) to their respective products. In **7a**, CCNN is 94.8°; in **8**, CCNN is 83.8°. Calculated by M06-2X/6-31+G(d) IEF-PCM: $CHCl_3$.

higher than experimental values. This is likely due to overestimation of $-T\Delta S^{\ddagger}$ for bimolecular reactions in solution. This is supported by the $\Delta H^{\ddagger}$ of enamines **1a** and **2** in Table 1 where M06-2X energetics agree quite closely with experimental barriers. Figure 8 shows the $\Delta G^{\ddagger}_{expt}$ vs $\Delta G^{\ddagger}_{comp}$ for the three methods used in this work. The discussion refers to the quantum mechanical results using the M06-2X functional.

Regioselectivities. The energetics for formation of the regioisomers were shown in Figure 6. The activation energies for formation of regioisomers **3a** and **5** are 11.2 and 7.6 kcal mol^{-1} lower, respectively, than that for formation of unobserved products **4a** and **6.** Previous studies by Munk et al. and Pocar et al. attempted to decrease the regioselectivity of the enamine−azide 1,3-dipolar cycloaddition by utilizing more sterically bulky enamines. Tetrasubstituted enamines were used as dipolarophiles, and only one regioisomer was formed in these studies because of the cited *electronic control* that results from the electron donation from the nitrogen.[23,24]

The distortion/interaction model developed by our group[10] has recently been used to explain the reactivities and selectivities of cycloadditions in bioorthogonal reactions,[25,26] materials chemistry,[27] and palladium-catalyzed cross-coupling reactions.[28] The distortion/interaction model dissects activation barriers ($\Delta E^{\ddagger}$) of bimolecular reactions into distortion energies ($\Delta E_d^{\ddagger}$) and interaction energies ($\Delta E_i^{\ddagger}$). The distortion energy is the amount of energy required to distort phenyl azide and the enamine into their transition state geometries without allowing the cycloaddition partners to interact. The interaction energy arises from a combination of closed-shell (steric) repulsion, charge transfer involving occupied and vacant orbital interactions, electrostatic interactions, and polarization effects. These results from the distortion/interaction analysis are shown in Table 2.

dx.doi.org/10.1021/jo302695n | J. Org. Chem. 2013, 78, 1576−1582

Table 1. Rate Constants Reported by Munk et al.[8] and the Derived $\Delta G^{\ddagger}_{expt}$ Values with Reported Errors[a]

enamine	$10^7 k_2$ (M^{-1} s^{-1})	$\Delta G^{\ddagger}_{expt}$ (kcal mol^{-1})	$\Delta H^{\ddagger}_{expt}$ (kcal mol^{-1})	$\Delta G^{\ddagger}_{M06\text{-}2X}$[c] (kcal mol^{-1})	$\Delta H^{\ddagger}_{M06\text{-}2X}$ (kcal mol^{-1})	$\Delta G^{\ddagger}_{SCS\text{-}MP2}$ (kcal mol^{-1})	$\Delta H^{\ddagger}_{SCS\text{-}MP2}$ (kcal mol^{-1})	$\Delta G^{\ddagger}_{B97d}$ (kcal mol^{-1})
1a	152	25.7 ± 1.2	15 ± 1.2	30.1	15.1	31.6	17.6	18.7
1b	33	26.6 ± 0.02[b]	–	31.1	–	31.8	–	19.8
1c	5167	23.4 ± 0.02[b]	–	27.9	–	28.8	–	16.7
2	1667	24.1 ± 1.2	13 ± 1.2	27.5	12.7	26.9	12.7	19.3

[a]$\Delta G^{\ddagger}$ computed using M06-2X/6-311+G(d,p), B97D/6-311+G(d,p), and SCS-MP2/6-311+G(d,p)//M06-2X/6-311+G(d,p) IEF-PCM: $CHCl_3$. Computed barriers carried at 44.8 °C to match experimental conditions. [b]Error bars were derived from the report that the maximum error was 1.0%. [c]Computed free energies in solution are for the standard state of 1M.[22]

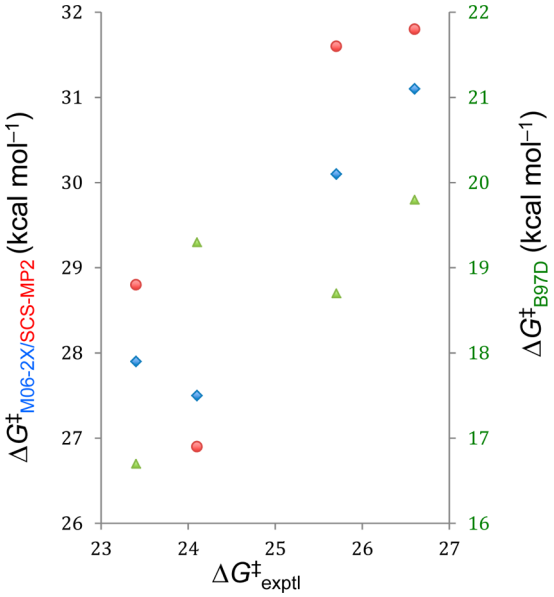

Figure 8. $\Delta G^{\ddagger}_{expt}$ values derived from experimental rate constants. $\Delta G^{\ddagger}_{comp}$ energies are computed in solvent using IEF-PCM ($CHCl_3$). The reactions of phenyl azide with dipolarophiles **1a–c** and **2** M06-2X/6-311+G(d,p) (blue diamond),SCS-MP2/6-311+G(d,p)//M06-2X/6-311+G(d,p) (red circle), and B97D/6-31G(d,p) (green triangle).

The distortion energy consists of azide distortion energy and dipolarophile distortion energy. The exclusive formation of **3a** from **1a** results from the lowest energy transition state, **TS(1a→3a)**. **TS(1a→4a)** has a higher energy primarily due to its 8.1 kcal mol^{-1} less favorable interaction energy. This arises from the more favorable HOMO–LUMO interaction as described in early FMO theories of cycloaddition regioselectivity.[29−32] Figure 9 shows the LUMO of the azide is concentrated at the unsubstituted N terminus. This becomes united with the nucleophilic terminus β to the N; this is the site of the largest HOMO coefficient. The $\Delta\Delta E_d^{\ddagger}$ is relatively small (3.0 kcal mol^{-1}); the interaction energy controls the reactivity. Distortion energies reinforce the preference controlled by the interaction energy, because the unfavorable transition state is later and more distorted from the equilibrium geometry.

The reaction of **2** with phenyl azide yields only **5**. $\Delta\Delta E_i^{\ddagger}$ is approximately equal (0.5 kcal mol^{-1}) for **TS(2→5)** and **TS(2→6)**. In this case, the favored product, **5**, is formed because of *distortion* energy control. The azide distortion energy is 4.5 kcal mol^{-1} higher in **TS(2→6)** than in **TS(2→5)**. As shown in Figure 9, the HOMO of **2** is quite high and the terminal alkene π coefficients are nearly the same. Both transition states have favorable interaction energies. Figure 4 shows that the phenyl group of phenyl azide is aligned with the azide in **TS(1a→3a)** and **TS(2→5)** but is bent 38° out of this plane in **TS(2→6)**. **TS(2→6)** allows favorable π stacking to occur, but this is unfavorable compared to the position of the phenyl group in **TS(2→5)**.

The polar nature of this reaction was thought to proceed through a charge-separated transition state. The high-lying enamine HOMO does indeed lead to significant charge transfer from the enamine to the azide. We calculated the charge separation in the solvent optimized transition states (ethanol and chloroform) using natural bond orbitals (NBO);[33] the results are listed in Table 3. The large charge separation is due to the relatively small HOMO–LUMO gap resulting from the high-lying HOMO of the enamine and the LUMO of phenyl azide. There appears to be a small solvent effect as compared to the gas phase for the greatly charge separated transition states, **TS(1a→3a)** and **TS(2→5)**, but the activation barriers are higher for the unfavored transition states in the gas phase. This result is consistent with the similar experimental rates determined by Munk et al. in chloroform and ethanol.[8]

Table 3 shows the significant charge separation for the favored (0.36–0.37e) and stepwise transition states (0.46–0.48e) and notably less for the disfavored transition states (0.06e–0.17e). The asynchronicities of the transition states are qualitatively correlated with the amount of charge separation in the transition state. The charge separation for **TS(1a→3a)** in both solvents is 0.37e indicative of a very polar transition state, whereas **TS(1a→4a)** has a charge separation of only 0.06e,

Table 2. M06-2X/6-311+G(d,p) IEF-PCM ($CHCl_3$): Electronic Activation ($\Delta E^{\ddagger}$) Energies, Distortion Energies ($\Delta E_d^{\ddagger}$), and Interaction Energies ($\Delta E_i^{\ddagger}$) for the Reactions of Phenyl Azide and Enamines 1a and 2

	$\Delta E^{\ddagger}$ (kcal mol^{-1})	$\Delta E_d^{\ddagger}$ total (kcal mol^{-1})	$\Delta E_d^{\ddagger}$ dipolarophile (kcal mol^{-1})	$\Delta E_d^{\ddagger}$ Azide (kcal mol^{-1})	$\Delta E_i^{\ddagger}$ kcal mol^{-1})
TS(1a→3a)	14.6	31.8	7.0	24.8	−17.3
TS(1a→4a)	25.6	34.8	9.8	25.0	−9.2
TS(1a→7a)	15.5	33.0	6.9	26.1	−17.6
TS(2→5)	11.8	30.0	6.6	23.4	−18.2
TS(2→6)	19.2	36.7	8.8	27.9	−17.6
TS(2→8)	16.5	34.6	7.9	26.7	−18.1

dx.doi.org/10.1021/jo302695n | J. Org. Chem. 2013, 78, 1576–1582

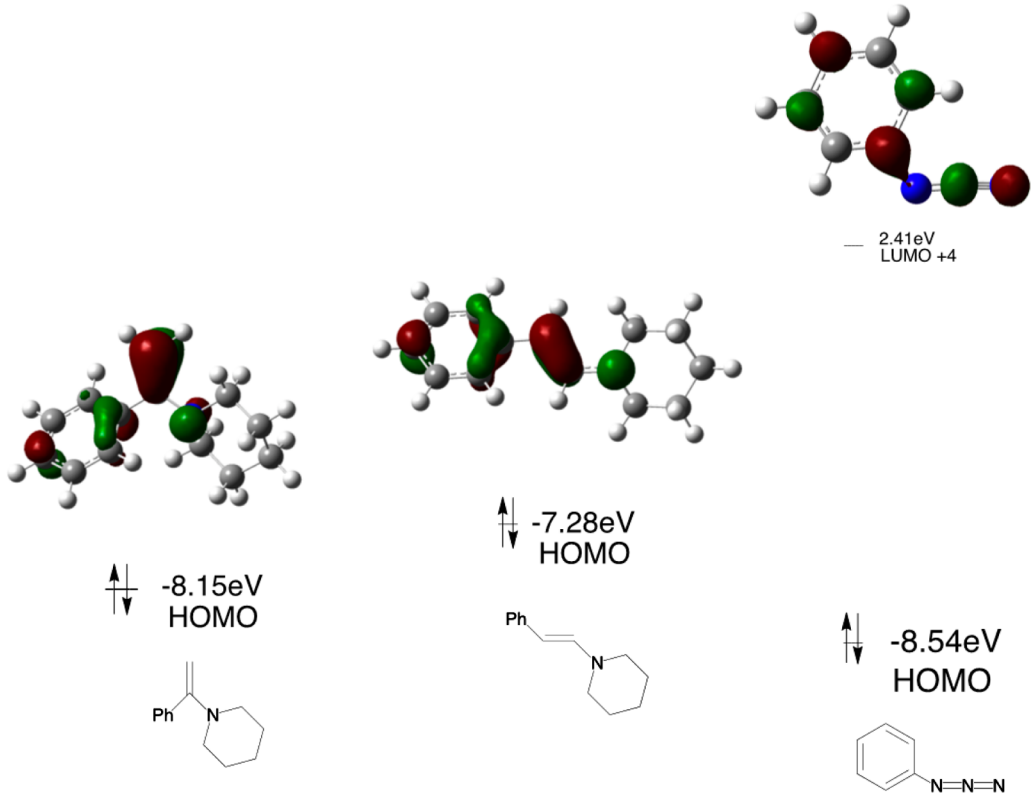

Figure 9. FMO diagram for the cycloadditions of **1a** and **2** with phenyl azide. HF/6-311+G(d,p)//M06-2X/6-311+G(d,p) computed orbital energies.

Table 3. $\Delta G^{\ddagger}$ and for the Three Possible Transition Structures and the Charge Separation (NBO) in the Transition Structures[a]

	$\Delta G^{\ddagger}_{GAS}$ (kcal mol^{-1})	$\Delta G^{\ddagger}_{CHCl_3}$ (kcal mol^{-1})	$\Delta G^{\ddagger}_{EtOH}$ (kcal mol^{-1})	charge separation ($CHCl_3$)	charge separation (EtOH)
TS(1a→3a)	32.4	29.8	29.8	0.37e	0.37e
TS(1a→4a)	42.9	41.0	41.1	0.06e	0.06e
TS(1a→7a)	–	30.9	30.6	0.46e	0.44e
TS(2→5)	30.1	27.2	27.0	0.36e	0.36e
TS(2→6)	36.1	34.8	35.2	0.17e	0.17e
TS(2→8)	–	31.7	31.1	0.48e	0.46e

[a]Values calculated by M06-2X/6-311+G(d,p) IEF-PCM: $CHCl_3$ and EtOH.

more similar to a normal unactivated alkene azide cycloaddition transition state.[34,35]

Cycloadditions of Pyrrolidine and Morpholine Enamines with Azides. Munk also investigated the cycloadditions of enamines consisting of morpholine and pyrrolidine. He states, "Although piperidine and pyrrolidine are nearly equal in basicity, the acetophenone enamine of the latter amine is 34 times more reactive toward phenyl azide. In sharp contrast the piperidine enamine reacts only 4.5 times faster than the morpholine enamine in spite of the 1000-fold difference in amine basicity."[8] The transition structures for these reactions [(**TS(1b→3b)** and **TS(1c→3c)**] are shown in Figure 10. As with **TS(1a→3a)** and **TS(2→5)**, the transition states are quite asynchronous [0.71 Å and 0.68 Å for **TS(1b→3b)**] and **TS(1c→3c)**, respectively)].

Munk et al. cite the superior resonance donation of the pyrrolidine versus piperidine to rationalize the greater reactivity of **1b** over **1a**.[36] Table 4 shows a small range of interaction energies (−17.6 to −16.3 kcal mol^{-1}), whereas the distortion energies have a larger range (28.7 to 33.0 kcal mol^{-1}). The

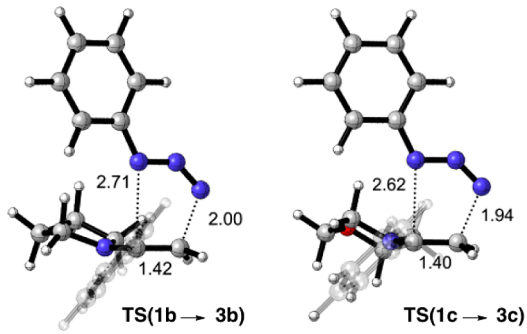

Figure 10. **TS(1b→3b)** and **TS(1c→3c)** with phenyl azide as calculated by M06-2X/6-311+G(d,p) using IEF-PCM: $CHCl_3$. Bond lengths are in Å, and the phenyl groups were made transparent for a clearer view of the transition states.

distortion energy controls the reactivity of the enamines **1a**, **1b**, and **1c**.

The sterically crowded environment of the 1,1-disubstituted enamines (**1a−c**) allows only one of the substituents to become

dx.doi.org/10.1021/jo302695n | J. Org. Chem. 2013, 78, 1576−1582

Table 4. $\Delta E^{\ddagger}$, $\Delta E_d^{\ddagger}$, $\Delta E_i^{\ddagger}$, and $\Delta G^{\ddagger}$ for the Morpholine and Pyrrolidine Enamine Cycloaddition Reactions with Phenyl Azide[a]

enamine	$\Delta E^{\ddagger}$ (kcal mol^{-1})	$\Delta E_d^{\ddagger}$ (kcal mol^{-1})	$\Delta E_i^{\ddagger}$ (kcal mol^{-1})	$\Delta G^{\ddagger}$ (kcal mol^{-1})	k_2 x 10^3 (L mol^{-1}min^{-1})
TS(1a→3a)	14.6	31.8	−17.3	29.8	0.91
TS(1b→3b)	12.4	28.7	−16.3	27.6	31.0
TS(1c→3c)	15.4	33.0	−17.6	30.7	0.20

[a]Calculated by M06-2X/6-311+G(d,p) IEF-PCM: $CHCl_3$.

planar with the double bond. The five-membered ring of pyrrolidine can planarize and give maximum overlap with a lower energy penalty than piperidine. **TS(1a→3a)** and **TS(1c→3c)** have nearly equivalent distortion energies (31.8 and 33.0 kcal mol^{-1}). **TS(1b→3b)** has reduced distortion energy (28.7 kcal mol^{-1}), which reflects the relative ease with which pyrrolidine is planarized to the transition state geometry.

CONCLUSION

We have found that the cycloadditions of enamines with phenyl azide are concerted reactions with asynchronous transition states. The frontier molecular orbital analysis provided insights into reactivities and regioselectivities. The distortion energy influences reactivtities of different enamines by the necessity of planarizing the amine in the transition state.

ASSOCIATED CONTENT

Supporting Information

Calculated geometries and energies with M06-2X and SCS-MP2 methods; solvation energies; complete ref 11 for Gaussian 09. This information is available free of charge via the Internet at http://pubs.acs.org.

AUTHOR INFORMATION

Corresponding Author

*E-mail: houk@chem.ucla.edu.

Notes

The authors declare no competing financial interest.

ACKNOWLEDGMENTS

We thank the National Science Foundation (NSF CHE-1059084) for financial support of this research. This work used computer time supplied by the Extreme Science and Engineering Discovery Environment (XSEDE), which is supported by National Science Foundation Grant No. OCI-10535

REFERENCES

(1) Kolb, H. C.; Finn, M. G.; Sharpless, K. B. *Angew. Chem., Int. Ed.* **2001**, *40*, 2004.
(2) Agard, N. J.; Prescher, J. A.; Bertozzi, C. R. *J. Am. Chem. Soc.* **2004**, *126*, 15046.
(3) Chang, P. V.; Prescher, J. A.; Sletten, E. M.; Basin, J. M.; Miller, I. A.; Agard, N. J.; Lo, A.; Bertozzi, C. R. *Proc. Natl. Acad. Sci. U.S.A.* **2010**, *107*, 1821.
(4) Karver, M. R.; Weissleder, R.; Hilderbrand, S. A. *Angew. Chem., Int. Ed.* **2012**, *51*, 920.
(5) Cao, Y.; Houk, K. N. *J. Mater. Chem.* **2011**, *21*, 1503.
(6) Kolb, H. C.; Finn, M. G.; Sharpless, K. B. *Angew. Chem., Int. Ed.* **2001**, *40*, 2004.
(7) Agard, N. J.; Prescher, J. A.; Bertozzi, C. R. *J. Am. Chem. Soc.* **2004**, *126*, 15046.
(8) Meilahn, M. K.; Cox, B.; Munk, M. E. *J. Org. Chem.* **1975**, *40*, 819.
(9) Jones, G. O.; Houk, K. N. *J. Org. Chem.* **2008**, *73*, 1333.
(10) Ess, D. H.; Houk, K. N. *J. Am. Chem. Soc.* **2007**, *129*, 10646.
(11) Frisch, M. J.; et al.*Gaussian 09*, revision C-01; Gaussian Inc.; Wallingford, CT, 2009 (see complete reference in the Supporting Information).
(12) Zhao, Y.; Truhlar, D. G. *Theor. Chem. Acc.* **2008**, *120*, 215.
(13) Grimme, S. *J. Comput. Chem.* **2006**, *27*, 1787.
(14) (a) Grimme, S. J. *J. Chem. Phys.* **2003**, *109*, 3067. (b) Grimme, S. *J. Chem. Phys.* **2003**, *118*, 9095. (c) Greenkamp, M.; Grimme, S. *Chem. Phys. Lett.* **2004**, *392*, 229.
(15) Tomsi, J.; Mennucci, B.; Cances, E. *THEOCHEM* **1999**, *464*, 211.
(16) Barone, V.; Cossi, M. *J. Phys. Chem.* **1998**, *102*, 1995.
(17) Cossi, M.; Rega, N.; Scalmani, G.; Barone, V. *J. Comput. Chem.* **2003**, *24*, 669.
(18) Zhao, Y.; Truhlar, D. G. *Phys. Chem. Chem. Phys.* **2008**, *10*, 2813.
(19) Ribeiro, R. F.; Marenich, A. V.; Cramer, C. J.; Truhlar, D. G. *J. Phys. Chem. B* **2011**, *115*, 14556.
(20) Huisgen, R.; Mloston, G.; Langhals, E. *J. Org. Chem.* **1986**, *51*, 4085.
(21) Quast, H.; Manfred, B.; Hergenroether, T.; Regnat, D.; Lehmann, J.; Banert, K. *Helv. Chim. Acta* **2005**, *88*, 1589.
(22) Vasquez, S.; Camps, P. *Tetrahedron* **2005**, *61*, 5147.
(23) Kim, Y. K.; Munk, M. E. *J. Am. Chem. Soc.* **1964**, *86*, 2213.
(24) Fusco, R.; Bianchetti, G.; Pocar, D. *Gazz. Chim. Ital.* **1961**, *91*, 849.
(25) Gordon, C. G.; Mackey, J. L.; Jewett, J. C.; Sletten, E.; Houk, K. N.; Bertozzi, C. R. *J. Am. Chem. Soc.* **2012**, *134*, 9199.
(26) Liang, Y.; Mackey, J. L.; Lopez, S. A.; Liu, F.; Houk, K. N. *J. Am. Chem. Soc.* **2012**, *134*, 17904.
(27) Cao, Y.; Houk, K. N. *J. Mater. Chem.* **2011**, *21*, 1503.
(28) Schoenebeck, F.; Houk, K. N. *J. Am. Chem. Soc.* **2010**, *132*, 2496.
(29) Houk, K. N. *J. Am. Chem. Soc.* **1972**, *94*, 8953.
(30) Houk, K. N.; Sims, J.; Duke, R. E., Jr.; Strozier, R. W.; George, J. K. *J. Am. Chem. Soc.* **1973**, *95*, 7287.
(31) Houk, K. N.; Sims, J.; Watts, C. R.; Luskus, L. J. *J. Am. Chem. Soc.* **1973**, *95*, 7301.
(32) Sustman, R.; Trill, H. *Angew. Chem., Int. Ed. Engl.* **1972**, *11*, 838.
(33) Foster, J. P.; Weinhold, F. *J. Am. Chem. Soc.* **1980**, *102*, 7211.
(34) Huisgen, R.; Szeimies, G.; Möbius, L. *Chem. Ber.* **1967**, *100*, 2494.
(35) Scheiner, P.; Schomaker, J. H.; Deming, S.; Libbey, W. J.; Novak, G. P. *J. Am. Chem. Soc.* **1965**, *87*, 306.
(36) Stork, G.; Brizzolara, A.; Landesman, H.; Szmuszkovicz, J.; Terrell, R. *J. Am. Chem. Soc.* **1963**, *85*, 207.